The benthic foraminiferal response to the mid-Maastrichtian event in the NW-European chalk sea of the Maastrichtian type area

Author for correspondence:
Iris Vancoppenolle,
Email: vancoppenolleiris@live.be

Iris Vancoppenolle[1] , Johan Vellekoop[1,2], Monika Doubrawa[1] , Pim Kaskes[3], Matthias Sinnesael[3,4], John W.M. Jagt[5], Philippe Claeys[3] and Robert P. Speijer[1]

[1]Department of Earth and Environmental Sciences, Division Geology, KU Leuven, Leuven, Belgium; [2]OD Earth and History of Life, Royal Belgian Institute of Natural Sciences, Brussels, Belgium; [3]Analytical, Environmental and Geo-Chemistry, Vrije Universiteit Brussel, Brussels, Belgium; [4]IMCCE, CNRS, Observatoire de Paris, PSL University, Sorbonne Université, Paris, France and [5]Natuurhistorisch Museum Maastricht, Maastricht, The Netherlands

Abstract

The mid-Maastrichtian carbon isotope event (MME), dated at ~69 Ma, reflects a perturbation of the global carbon cycle that, in part, correlates with the enigmatic global extinction of 'true' (i.e., non-tegulated) inoceramid bivalves. The mechanisms of this extinction event are still debated.

While both the inoceramid extirpation and MME have been recorded in a variety of deep-sea sites, little is known about their expression in epicontinental chalk seas. In order to study the shallow-marine signature of the MME in this epicontinental shelf sea, we have generated quantitative foraminiferal assemblage data for two quarries (Hallembaye, NE Belgium; ENCI, SE Netherlands) in the Maastrichtian type area, complemented by a species-specific benthic $\delta^{13}C$ record. In contrast to deep-sea records, no significant changes in benthic foraminiferal assemblages and benthic foraminiferal accumulation rates are observed across the MME in the type-Maastrichtian area. At the Hallembaye quarry, the otherwise rare endobenthic species *Cuneus trigona* reaches a transient peak abundance of 33.3% at the onset of the MME, likely caused by a local transient change in organic matter flux to the seafloor. Nevertheless, high and near-constant species evenness shows that neither oxygen nor organic matter flux was limited across the extinction level or during the MME. Benthic foraminiferal data from the uppermost part of the studied section, above the MME, indicate a significant increase in food supply to the seafloor. Decreased amounts of terrigenous elements across this interval document a lesser riverine or aeolian influx, which means that the increased benthic productivity is linked to a different origin. Potentially, the continuous precipitation of chalk under nutrient-poor conditions in the Late Cretaceous chalk sea was enabled by efficient nutrient recycling in the water column. In shallower depositional settings, nutrient recycling took place closer to the seafloor, which allowed more organic matter to reach the bottom. These results provide insights in the importance of nutrient cycling for biological productivity in the NW-European chalk sea.

CAMBRIDGE UNIVERSITY PRESS

Introduction

Inoceramid bivalves (Pteriomorpha, Inoceramidae) constituted a dominant epibenthic component of seafloor communities during the Cretaceous Period (145–66 Ma), with broad ecological tolerances and a near global distribution, until they experienced a rapid decline in the mid-Maastrichtian (~69 Ma; MacLeod et al., 1996). After a short-lived peak abundance in the early Maastrichtian nearly all inoceramid species, with the exception of the enigmatic genera *Spyridoceramus* and *Tenuipteria*, went extinct (MacLeod et al., 1996; Chauris et al., 1998; Jagt & Jagt-Yazykova, 2018).

While the extinction of 'true' (i.e., non-tegulated) inoceramids was diachronous (Chauris et al., 1998), the decline of this ubiquitous fossil group has generally been linked to environmental changes during the mid-Maastrichtian, possibly reflected by the mid-Maastrichtian carbon isotope event (MacLeod et al., 1996; Gómez-Alday et al., 2004; Friedrich & Hemleben, 2007; Jung et al., 2013; see Fig. 1). The mid-Maastrichtian event (MME) comprises two $\delta^{13}C$ maxima (MME1 and MME3) with a negative ~0.5 permille $\delta^{13}C$ excursion in between (MME2; Voigt et al., 2012), signifying a perturbation of the global carbon cycle. This perturbation appears to coincide approximately with the enigmatic global extinction of 'true' inoceramids (Frank et al., 2005; Huber et al., 2008), suggesting a potential causal relationship. On the basis of benthic and planktic foraminiferal $\delta^{13}C$ and $\delta^{18}O$ data and Nd-isotope records from sites in the Pacific, Southern and Atlantic oceans, the hypothesis has been put forward that the extirpation of inoceramids was caused by a reorganisation of the deep ocean circulation (MacLeod, 1994; MacLeod et al., 1996; Barrera et al., 1997; Frank & Arthur, 1999; Frank et al., 2005;
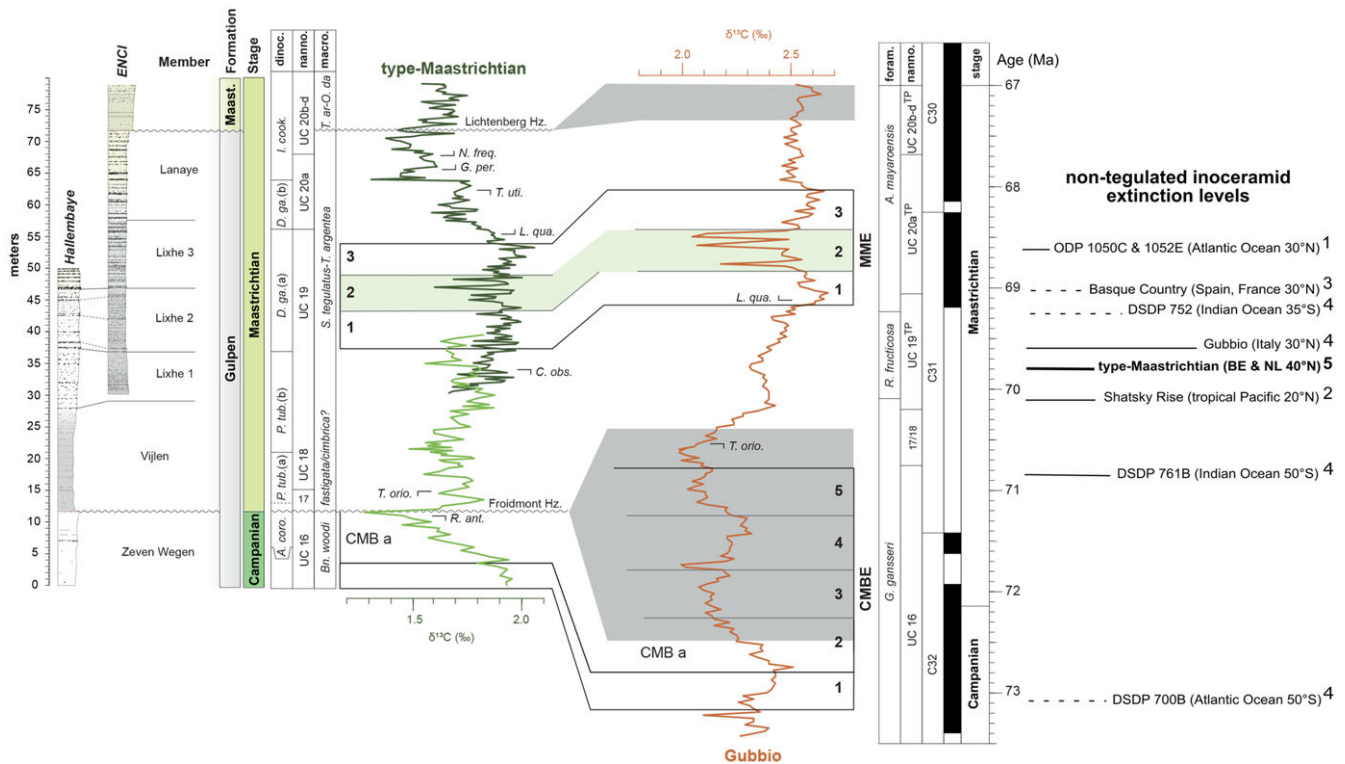
Fig. 1. Correlation of the type-Maastrichtian δ¹³C record (Vellekoop et al., 2022) to the age-scaled δ¹³C record for Gubbio (Voigt et al., 2012; age reassigned by Batenburg et al., 2018a), plotted alongside inoceramid extinction levels at different sites. Full lines mark extinction levels that are relatively well constrained in time, while those less well constrained are indicated by dotted lines. Image is based on Vellekoop et al. (2022). Inoceramid extinction references are as follows: [1]MacLeod & Huber (2001; age reassignment by Huber et al., 2008); [2]Dameron et al. (2017); [3]Gómez-Alday et al. (2004) and Batenburg et al. (2014); [4]Chauris et al. (1998); [5]Walaszczyk et al., (2010; age reassignment by Vellekoop et al., 2022). Dinoc. = dinocysts, Macro. = macrofossil, Nanno. = nannofossil, Foram. = planktic foraminifera stratigraphy. A. coro. = Areoligera coronat, P. tub. = Pervosphaeridium tubuloaculatum, D. ga. = Deflandrea galeata, I. cook. = Isabellidinium Cooksoniae, CMBE = Campanian–Maastrichtian Boundary Event, MME = mid-Maastrichtian carbon isotope event.

Friedrich & Hemleben, 2007; MacLeod et al., 2011; Koch & Friedrich, 2012). During the Maastrichtian, the formation of intermediate to deep water would have gradually shifted from a saline and warm low-latitude origin towards a dominant cool, less saline, well-oxygenated high latitude source area (MacLeod et al., 1996; Friedrich & Hemleben, 2007), leading to a gradual intensification of deep water circulation (Batenburg et al., 2018a). Assuming that early Maastrichtian inoceramids generally preferred warm, low-oxygen conditions, which is supported by distribution data (MacLeod, 1994), the gradual shift towards oxygen-rich intermediate and deep water formation could explain the diachronous character of their extinction (MacLeod, 1994; MacLeod et al., 1996). The Shatsky Rise (tropical Pacific) was briefly colonised by inoceramids prior to the extinction event; this coincides with the onset of the MME and is marked by a collapse of the δ¹³C gradient between surface and bottom waters, an increase in the relative abundance of biserial planktic foraminifera, and a sharp decrease in benthic δ¹⁸O values, which are interpreted to document an increase in productivity and higher seafloor temperatures (Frank et al., 2005, Jung et al., 2013). Variations in the relative abundance of epibenthic *vs* endobenthic foraminifera suggest variable organic matter fluxes to the ocean floor (Frank et al., 2005; Dameron et al., 2017). However, it remains unclear how organic fluxes to the ocean floor changed, because there are few records with quantitative benthic foraminiferal assemblage data, and those that are available (Frank et al., 2005; Dameron et al., 2017) show conflicting signals, highlighting the importance of additional benthic foraminiferal records across the MME. The North Atlantic shows an increase

in both δ¹³C gradient and planktic foraminiferal diversity across the mid-Maastrichtian, indicating increased stratification (MacLeod et al., 2005). Frank et al. (2005) proposed that the source of intermediate water in the tropical Pacific changed during the MME, from having a predominantly North Pacific origin to a predominantly Southern Ocean origin, with transient intermediate water fluxes from the western Tethys, leading to the short-lived colonisation by inoceramids. In contrast, Jung et al. (2013) suggested that in the tropical Pacific the MME reflected a weakening of the Southern Ocean deep water advection, thereby ending the intensified deep ocean circulation of the early Maastrichtian and briefly (~1 Myr) returning to a Campanian circulation mode during the late Maastrichtian. Based on Nd-isotope records, MacLeod et al. (2011) suggested that the MME reflected the onset or intensification of intermediate and deep water formation in the North Atlantic, one of the major drivers of circulation in present-day oceans. Model studies indicate that a region of deep water formation might have existed along the North American shelfs during the mid-Maastrichtian (Donnadieu et al., 2016).

Regardless of the driving mechanisms, the demise of inoceramids, with their wide ecological and geographical range, is suggestive of a major perturbation in benthic ecosystems. However, the ultimate cause of the extinction of the inoceramids is still debated, as we do not understand which physiochemical and ecological changes took place on the seafloor and whether or not the δ¹³C excursion was related to the extinction event.

While both the decline of inoceramids and the MME have been recorded in a variety of deep-sea sites, few studies have focused on

the relatively shallow epicontinental chalk seas (Dubicka & Peryt, 2012). Moreover, many aspects of these chalk seas are not yet fully understood, including productivity, oxygenation and nutrient cycling. The chalk seas, characterised by dominant production of chalk and regular formation of flint beds, are thought to have been a stable environment with low upper water column productivity; this is supported by palynofacies and nannofossil data (Sheldon et al., 2010; and references therein). Possibly, efficient recycling of nutrients was prevalent in the upper water column, which allowed the continuous precipitation of chalk by calcareous nannoplankton, under nutrient-poor conditions. Alternatively, inflow of nutrient-rich intermediate water from the North Atlantic could have provided the European chalk sea with nutrients (Friedrich et al., 2005; Engelke et al., 2017). Although the Late Cretaceous chalk sea might have been characterised by relatively low primary productivity in the photic zone, sea floor productivity could still have been comparatively high, due to the presence of sponges, similar to modern coral reefs that thrive in nutrient-poor seas (de Goeij et al., 2013). Sponges efficiently capture dissolved organic matter and release particulate detritus, which is then consumed by other organisms, such as benthic foraminifera, resulting in effective recycling of nutrients on the seafloor. Although sponge fossils may be rare to absent in the Upper Cretaceous chalk, siliceous sponges were probably quite common, because they are thought to have been the main source of silica (Si) for the formation of flints (Jurkowska & Świerczewska-Gładysz, 2020; and references therein).

One example of such a shallow, epicontinental chalk sea is that of the carbonate platform successions in the Maastrichtian type area in the Belgium-Netherlands border region near the cities of Liège (BE) and Maastricht (NL). Recently, the stratigraphic position of the MME in this area was constrained by bulk carbonate $\delta^{13}C$ records from these successions (Fig 1; Vellekoop et al., 2022). The MME has been identified at two quarries (Hallembaye and the nearby ENCI; Figs. 2 and 3), in the upper part of the Lixhe 2 Member and lower part of the Lixhe 3 Member of the Gulpen Formation. 'True' inoceramids are quite rare in these sequences, but their highest occurrence is around 12 m below the initiation of the MME, near the top of the Vijlen Member of the Gulpen Formation (Walaszczyk et al., 2010). This succession therefore provides an opportunity to study whether or not the inoceramid extinction event and/or the MME in shallow epicontinental chalk seas is characterised by perturbations in the local benthic environment.

For the present study, quantitative foraminiferal assemblage data and a species-specific benthic $\delta^{13}C$ record have been generated to examine the shallow-marine signature of the MME. This has been done by using a subset of samples derived from the high-resolution sample set (5 cm sample spacing) recovered from the ENCI and Hallembaye quarries within the context of the Maastrichtian Geoheritage Project (Vellekoop et al., 2019, 2022).

Mid-Maastrichtian event

In the literature, the term 'MME' has been used in different ways. It was initially used to describe the extinction event of 'true' inoceramid bivalves (MacLeod et al., 1996; Frank & Arthur, 1999; Frank et al., 2005; Huber et al., 2008; Koch & Friedrich, 2012). However, this extinction event appears to have been highly diachronous (Chauris et al., 1998), with inoceramids apparently disappearing earlier in southern high latitudes and nearshore sites (MacLeod et al., 1996). It has been dated at ~69 Ma, just above the base of

Chron C31n, in the Basque region (Spain and France, Gómez-Alday et al., 2004; Batenburg et al., 2014), at 70.1 Ma in the northwest Pacific (Dameron et al., 2017) and between 68.5 and 68.7 Ma, just above the base of Chron C31n, in the western North Atlantic (MacLeod & Huber, 2001; age reassignment by Huber et al., 2008; see Fig. 1).

The term 'MME' has also been used to indicate a global carbon isotope event (Voigt et al., 2012; Jung et al., 2013). Voigt et al. (2012) defined the MME as a high $\delta^{13}C$ plateau consisting of a lower and upper maximum with a negative inflection in between. Those authors labelled the first maximum MME1, the second maximum MME3 and the decrease in between MME2. The MME starts just above the base of Chron C31n (Voigt et al., 2012). Using the age-scaled $\delta^{13}C$ record for Gubbio which encompasses the MME (Voigt et al., 2012 and references therein; ages reassigned by Batenburg et al., 2018b) the duration and ages of the different intervals of the MME can be estimated. MME1 is estimated to have started at ~69.2 Ma, MME2 at 68.8 Ma, MME3 at 68.4 Ma and the MME to have ended at ~68.0 Ma. Each MME interval has a duration of approximately 0.4 Myr. Others have used different labels for the main negative isotope excursion MME2. For example, Thibault et al. (2012) referred to the main negative MME excursion as M3-(a). In the present study, the term 'MME' is used to refer to the sequence of stable carbon isotope excursions as defined by Voigt et al. (2012).

Geological setting and stratigraphy

As a result of the high global sea level during the Late Cretaceous, large parts of Europe were covered by extensive, shallow epicontinental seas (Hancock, 1989); the Maastrichtian type area represents such a shelf sea (Fig. 2), situated between the Ruhr Valley Graben to the northeast and the Ardenno-Rhenish Massif to the southeast and at a palaeolatitude of ~40°N (van Hinsbergen et al., 2015). Sea level variations and tectonic rotational movements parallel to the NW-SE striking faults in the Ruhr Valley Graben resulted in lateral variations in lithology and stratigraphy in the Upper Cretaceous (middle Santonian-upper Maastrichtian) deposits in this area (Robaszynski et al., 1985). The rate of subsidence was highest in the southwest during the early Maastrichtian and in the northeast during the late Maastrichtian (Robaszynski et al., 1985).

Stratigraphical setting

The Hallembaye quarry (Fig. 3A), the former CPL SA-Haccourt quarry, is situated close to Haccourt in the province of Liège (Belgium). The ENCI quarry (Fig. 3B) lies south of Maastricht in the province of South-Limburg (the Netherlands). The ENCI quarry grounds include the type locality of the Maastrichtian Stage, introduced in 1849 by the Belgian geologist André Hubert Dumont (Jagt, 2001).

The Maastrichtian sequence of the type area comprises (parts of) three formations: the Gulpen Formation and overlying Maastricht and Kunrade formations. The present study concentrates on the Gulpen Formation, because this unit encompasses the lower-upper Maastrichtian transition (Vellekoop et al., 2022). It consists of chalk with abundant flint layers in the higher part of the unit and is subdivided into seven members, in ascending order: the Zeven Wegen, Beutenaken, Vijlen, Lixhe 1, Lixhe 2, Lixhe 3 and Lanaye Members (Felder, 1983; Fig. 3).
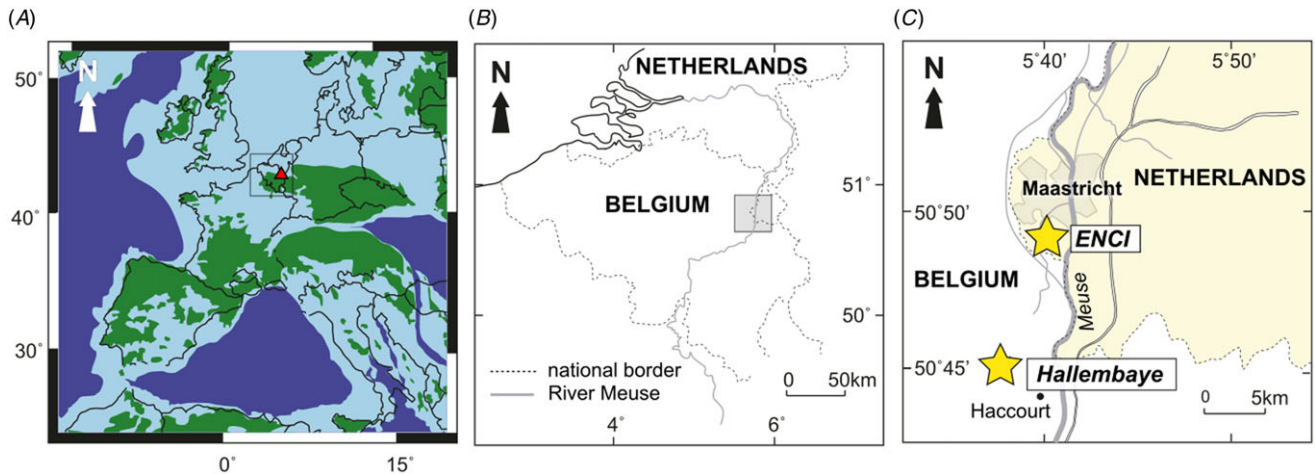
Fig. 2. (A) Paleogeographical setting of the type-Maastrichtian during the Maastrichtian, after Vellekoop et al. (2022): open ocean in dark blue; shelf seas in light blue; landmasses in green. (B) Geographic location of the Maastrichtian type area in the Netherlands-Belgium border region. (C) ENCI and Hallembaye quarries.
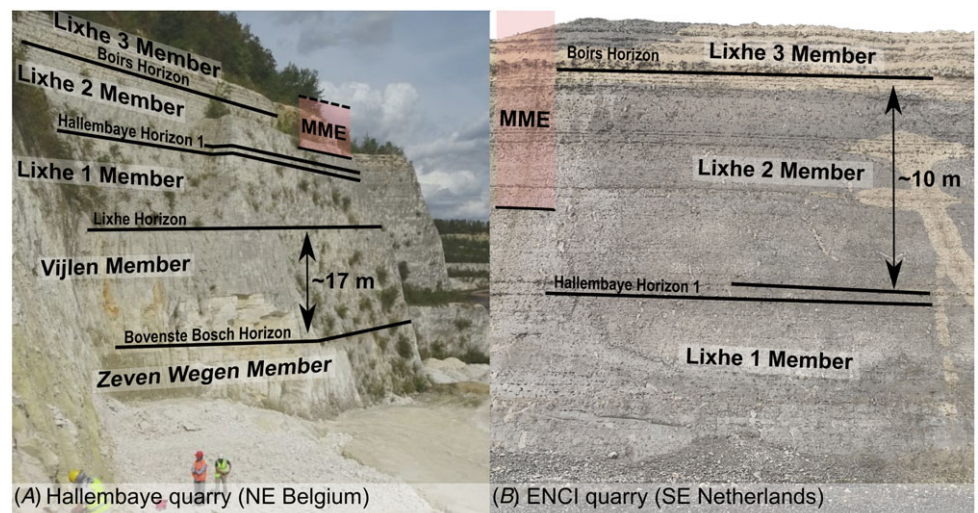

Fig. 3. Sections exposed (in part) at the Hallembaye (A) and ENCI quarries (B), with members and horizons marked.

The lower two units, the Zeven Wegen and Beutenaken members, are late Campanian in age (Felder, 1975). The remainder of the Gulpen Formation (i.e., from the Vijlen Member upwards) is Maastrichtian in age (Felder, 1975; Jagt & Jagt-Yazykova, 2012) and is the focus of this study. At Hallembaye, deposition of the Vijlen and Lixhe members took place in a relatively offshore setting and under low-energy conditions at an estimated palaeodepth of 80–100 m (Robaszynski et al., 1985). The Lanaye Member formed in a shallower environment with an estimated depth of 40–80 m (Jagt & Jagt-Yazykova, 2012).

The Vijlen Member has been interpreted as the infill of a channel system that eroded during the late Campanian or early Maastrichtian (Felder & Bless, 1994) in a relatively flat nearshore area with large, parallel channels extending from Aachen to Gulpen and from Altembroeck to Lanaye (Keutgen et al., 2010). The sediments consist of fine-grained glauconitic chalk with an upwards increasing $CaCO_3$ content, from ~50 to ~90% (Felder & Bosch, 2000; Vellekoop et al., 2022). Near the top, small light grey flint nodules occur. The Vijlen Member is rich in macrofossils, mainly brachiopods, bivalves, echinoids, inoceramids and belemnites (Robaszynski et al., 1985; Walaszczyk et al., 2010). Only the upper part of the member, containing flint nodules, is present at

the Hallembaye quarry; this is also found in boreholes in the subsurface at the former ENCI quarry (Felder & Bosch, 2000; Fig. 3A).

The Lixhe Horizon, which is the first (i.e., lowest) continuous, black flint layer, separates the Vijlen Member from the overlying Lixhe 1 Member. The latter consists of very fine-grained chalk with common dark grey to black flint nodules. The $CaCO_3$ content of the chalk, excluding the flint nodules, generally varies between 80 and 95% (Felder & Bosch, 2000; Vellekoop et al., 2022). The Lixhe 1 Member is also rich in macrofossils, mainly brachiopods and echinoids (Felder, 1983; Robaszynski et al., 1985). The top part of the Lixhe 1 Member comprises the '*Echinocorys* Level', a fossiliferous band with abundant echinoid tests that has been used as a marker bed in correlations of Maastrichtian strata across northern Europe (Dubicka & Peryt, 2012). The Lixhe 1 Member is exposed at both quarries (Felder & Bosch, 2000; Fig. 3).

The Lixhe 2 Member is separated from the Lixhe 1 Member by the Hallembaye Horizon 1, which is the lower of two continuous flint bands that can be traced throughout the Maastrichtian type region (Robaszynski et al., 1985). The Lixhe 2 Member consists of very fine-grained chalk with abundant dark grey to black flint nodules partly organised in layers. The $CaCO_3$ content of the chalk, excluding the flint nodules, varies between 80 and 95% (Felder &

Table 1. Sample list for the ENCI quarry with preservation state indicated.

Sample name	Height (m)	Member	Preservation[a]	Dry sample weight (g)	Split	Total benthic count	Isotope analysis	Assemblage data
ENCI_19_E_5.00	38.8	Lanaye	P	23.40	1/64	315		X
ENCI_19_E_3.00	36.8	Lanaye	P	24.80	1/64	375		X
ENCI_19_E_1.00	34.8	Lanaye	M	20.19	1/64	500	X	X
ENCI_19_D_3.00	32.8	Lanaye	M	26.35	1/32	310	X	X
ENCI_19_D_1.00	30.8	Lanaye	M	30.48	1/64	291	X	X
ENCI_19_C_2.00	28.3	Lanaye	P	30.05	1/64	413	X	X
ENCI_19_B_11.00	26.3	Lixhe 3	VP	30.03	1/64	457		X
ENCI_19_B_9.00	24.3	Lixhe 3	M	30.57	1/32	299	X	X
ENCI_19_B_8.00	23.3	Lixhe 3	P	25.50	1/32	310		X
ENCI_19_B_7.00	22.3	Lixhe 3	M	30.07	1/16	186	X	X
ENCI_19_B_5.00	20.3	Lixhe 3	VP	30.35	1/32	216	X	X
ENCI_19_B_4.00	19.3	Lixhe 3	VP	30.03	1/16	309		X
ENCI_19_B_3.00	18.3	Lixhe 3	VP	30.91	1/16	242	X	X
ENCI_19_A_16.00	16.3	Lixhe 2	P	30.75	1/8	272	X	X
ENCI_19_A_15.00	15.3	Lixhe 2	M	30.08	1/8	617		X
ENCI_19_A_14.00	14.3	Lixhe 2	VP	30.39	1/8	289	X	X
ENCI_19_A_12.00	12.3	Lixhe 2	VP	30.25	1/4	179	X	X
ENCI_19_A_11.00	11.3	Lixhe 2	P	29.25	1/8	402		X
ENCI_19_A_10.00	10.3	Lixhe 2	VP	30.83	1/4	245	X	X
ENCI_19_A_9.00	9.3	Lixhe 2	VP	30.15	1/8	237		X
ENCI_19_A_8.00	8.3	Lixhe 2	VP	30.30	1/4	262	X	X
ENCI_19_A_6.00	6.3	Lixhe 1	P	30.29	1/8	200	X	X
ENCI_19_A_4.00	4.3	Lixhe 1	VP	30.02	1/4	437		X
ENCI_19_A_2.00	2.3	Lixhe 1	VP	29.86	1/4	227	X	X
ENCI_19_A_0.00	0.3	Lixhe 1	VP	30.67	1/4	291		X

[a]M (moderate): some broken or dissolved, some recrystallisation and overgrowth; P (poor): most broken or dissolved, some recrystallisation and overgrowth; VP (very poor): most broken or dissolved, clear recrystallisation and overgrowth.

Bosch, 2000; Vellekoop et al., 2022). The chalk is poor in macro-fossils, mostly belemnites and echinoids (Felder, 1983; Robaszynski et al., 1985). This member is exposed at both quarries (Felder & Bosch, 2000; Fig. 3).

The Lixhe 3 Member is separated from the Lixhe 2 Member by the Boirs Horizon, which is the base of a ~50 cm thick continuous flint band. This unit consists of very fine-grained chalk with many small and large dark grey to black flint nodules, predominantly organised in layers. The CaCO$_3$ content of the chalk, excluding the flint nodules, varies from 90 to 97% (Felder & Bosch, 2000; Vellekoop et al., 2022). This member is comparatively poor in macrofossils; belemnites and bivalves, as well as a partial mosasaur skeleton, have been recorded to date (Felder, 1983; Bastiaans et al., 2020). It is exposed at both quarries (Felder & Bosch, 1998; Felder & Bosch, 2000; Fig. 3).

The base of the Lanaye Member is defined by the Nivelle Horizon, which is the middle of a conspicuous chalk layer below the lowest thick continuous flint level (Felder & Bosch, 1998, 2000). The Lanaye Member is separated from the overlying Maastricht Formation by the Lichtenberg Horizon, which is marked by a distinctly bioturbated layer at the top of the

Gulpen Formation, and a coarse grained, glauconite-rich, bioclastic sand layer rich in faecal pellets, at the base of the Maastricht Formation (Jagt & Jagt-Yazykova, 2012). The Lanaye Member comprises fine-grained chalk with many thick flint layers. The CaCO$_3$ content, excluding the flint nodules, equals ~95% (Vellekoop et al., 2022). This unit is rich in macrofossils, mainly echinoids, crinoids, bivalves, brachiopods and belemnites (Felder, 1983). It is exposed in its entirety only at the former ENCI quarry; at Hallembaye only the lower portion is available (Fig. 3B).

Position of the MME in the Maastrichtian type area

In the present study, we apply the revised age model for this succession as recently proposed by Vellekoop et al. (2022), on the basis of high-resolution bulk δ^{13}C stratigraphy, calibrated with nannofossil, dinoflagellate and belemnite biozonations.

The positions of the MME1, MME2 and MME3 at the Hallembaye and ENCI quarries have been determined by the bulk δ^{13}C signature (Fig 1; Vellekoop et al., 2022). This isotope record encompasses the MME at the ENCI quarry, and by

Table 2. Sample list for the Hallembaye quarry with preservation state indicated.

Sample name	Height (m)	Member	Preservation[a]	Dry sample weight (g)	Split	Total benthic count	Isotope analysis	Assemblage data
HAL18-B-48.50	48.50	Lixhe 3	VP	31.13	1/16	341		X
HAL18-A-46.50	46.50	Lixhe 3	P	30.70	3/16	213		X
HAL18-A-44.50	44.50	Lixhe 2	VP	33.48	1/32	207		X
HAL18-A-42.50	42.50	Lixhe 2	VP	30.76	3/32	253		X
HAL18-A-40.50	40.50	Lixhe 2	VP	30.70	1/16	222		X
HAL18-A-38.50	38.50	Lixhe 2	VP	30.54	1/8	292		X
HAL18-A-36.50	36.50	Lixhe 1	M	30.31	1/8	258		X
HAL18-A-34.50	34.50	Lixhe 1	P	30.50	1/8	235		X
HAL18-A-32.50	32.50	Lixhe 1	M	30.32	47/512	273		X
HAL18-A-30.50	30.50	Lixhe 1	P	30.39	1/8	186		X
HAL18-A-28.50	28.50	Lixhe 1	M	30.28	1/4	234		X
HAL18-A-26.50	26.50	Vijlen	P	31.31	1/16	240		X
HAL18-A-24.50	24.50	Vijlen	P	30.70	1/16	147		X
HAL18-A-22.50	22.50	Vijlen	M	31.24	1/16	180		X
HAL18-A-20.50	20.50	Vijlen	VP	30.50	1/32	98		X

[a]M (moderate): some broken or dissolved, some recrystallisation and overgrowth; P (poor): most broken or dissolved, some recrystallisation and overgrowth; VP (very poor): most broken or dissolved, clear recrystallisation and overgrowth.

lithostratigraphical correlation between both quarries the position of the MME can also be assessed at the Hallembaye quarry. All three parts of the MME are exposed at the ENCI quarry, while at the Hallembaye quarry only MME1 and part of MME2 are present.

The base of the MME is situated within the Lixhe 2 Member, approximately 12 m above the inoceramid extinction level which is located near the top of the Vijlen Member (Walaszczyk et al., 2010).

Material and methods

A total of 15 samples from the Hallembaye quarry, representing four members: Vijlen (4), Lixhe 1 (5), Lixhe 2 (4) and Lixhe 3 (2), have been studied, and 25 from the ENCI quarry, also representing four members: Lixhe 1 (4), Lixhe 2 (8), Lixhe 3 (7) and Lanaye (6), are studied. A sample spacing of 1–2.5 m has been used (see Tables 1 and 2).

Approximately 30 g of dry sediment was weighed of each sample and subsequently disaggregated by soaking in tap water, after which the residue was wet sieved to obtain fractions of 63 μm– 2 mm. After drying the residue at 40°C in an oven, it was dry sieved into three fractions: 630 μm–2 mm, 125–630 μm and 63–125 μm. The present study focuses on the 125–630 μm size fraction, because this allows sufficient precision for studying environmental perturbations, while also limiting processing time (Ernst et al., 2006; Weinkauf & Milker, 2018). Each sample was split with an ASC microsplitter until it contained around 250 benthic foraminifera. All benthic and planktic foraminifera were picked from this split and stored in Plummer slides.

The benthic foraminifera were identified at the genus or species level, following Frenzel (2000). The benthic foraminiferal number (BFN), i.e. the number of benthic foraminifera per gram of dry sediment, was also calculated. The benthic foraminiferal accumulation rate (BFAR, expressed in $cm^{-2}ky^{-1}$) was calculated by

multiplying BFN with the dry density of the chalk and with the carbonate sedimentation rate. The dry density of the chalk was estimated at 1.79 g/cm^3 (Bloomfield et al., 1995). The sedimentation rates were estimated using the age model by Vellekoop et al. (2022) and were in the order of 1.5–3.0 cm/ky. Benthic foraminiferal Shannon H diversity (H(S)) was calculated using the equation of Shannon & Weaver (1949) and species evenness (E) is measured by the Pielou's evenness index (Pielou, 1965).

The stable carbon isotopic composition of the benthic species *Cibicidoides bembix* was measured in order to obtain a species-specific benthic $\delta^{13}C$ record of the ENCI quarry. This species was chosen because it is abundant in all samples and thick-walled, making it in principle less susceptible to dissolution and recrystallisation. On the basis of overall test shape, it is thought to have led epibenthic lifestyle (i.e., living on top of the sediment; Frenzel, 2000). Therefore, its carbon isotope values are expected to reflect the signal of the bottom water.

For stable oxygen and carbon isotope analyses, around 10 specimens of *C. bembix* were picked from each sample, so as to obtain around 50 μg per sample. $\delta^{13}C$ and $\delta^{18}O$ values were measured in the isotope ratio mass spectrometer (IRMS) laboratory of the Analytical and Environmental Geo-Chemistry (AMGC) research group at the Vrije Universiteit Brussel (Brussels, Belgium; VUB). Samples were allowed to react with 104% phosphoric acid (H_3PO_4) at 70°C in a Nu-Carb carbonate preparation device and $\delta^{18}O$ and $\delta^{13}C$ were measured using a NuPerspective IRMS (Nu Instruments Ltd, Wrexham, UK). All isotope values are reported in ‰, relative to the Vienna Pee Dee Belemnite standard (‰ V-PDB). Calibration to the V-PDB standard via NBS-19 was made using the in-house Marbella limestone standard (MAR 2-2, +3.41‰ V-PDB $\delta^{13}C$, −0.13‰ V-PDB $\delta^{18}O$). Based on replicate measurements of MAR 2-2, one standard deviations were typically smaller than 0.1 for both $\delta^{18}O$ and $\delta^{13}C$.

For chemically well-preserved foraminifera, the $\delta^{13}C$ composition is a proxy for trophic conditions, whereas the $\delta^{18}O$ values
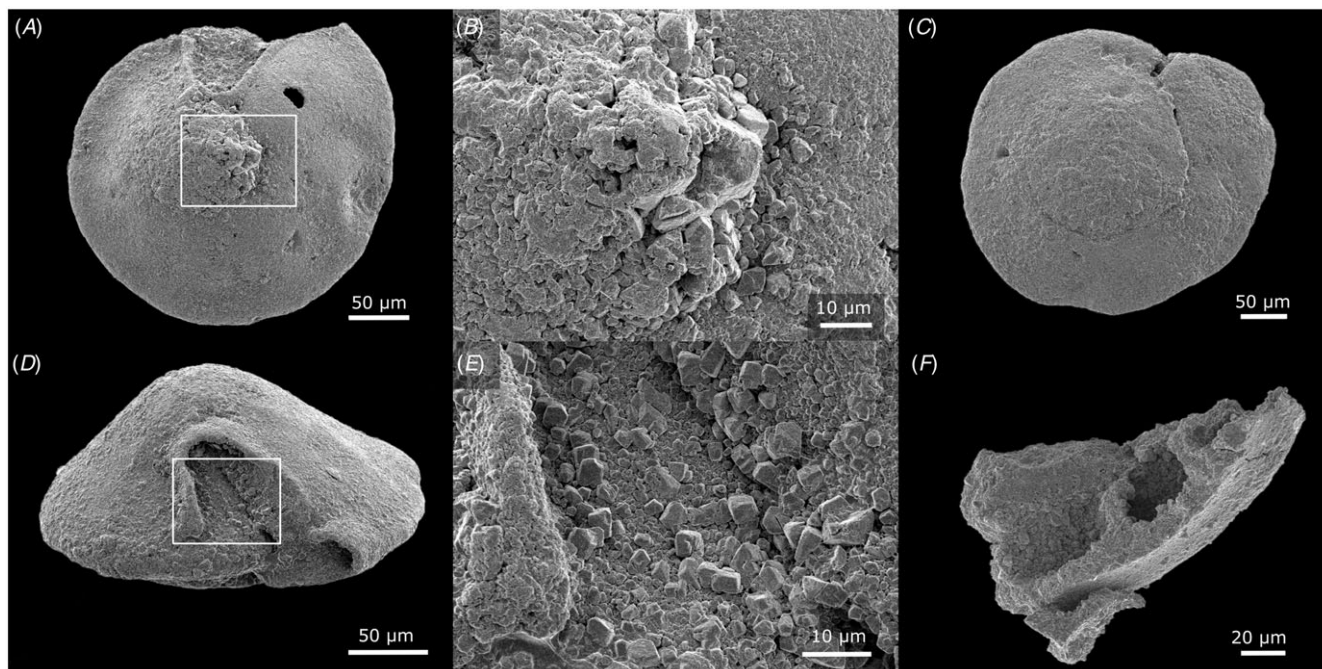
Fig. 4. Photomicrographs of Cibicidoides bembix, spiral view (A), detail of spiral view (B), umbilical view (C), apertural view (D), detail of apertural view (E), broken specimen shows recrystallisation and internal and external overgrowth, but no infilling (F). The specimens in this figure are from sample ENCI_19_B_9.00 (Lixhe 2 Member).
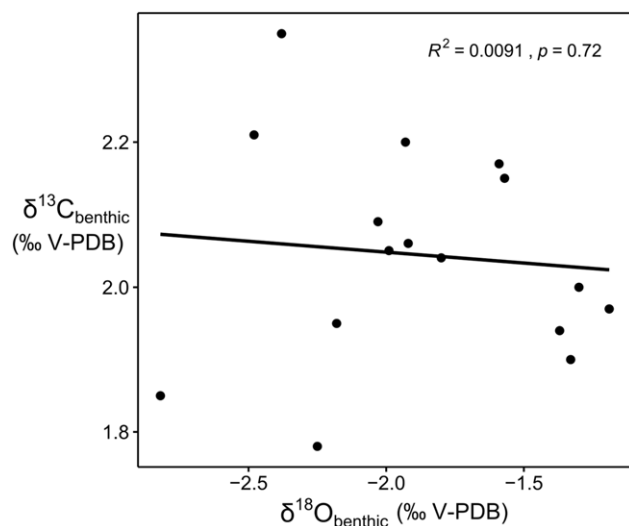

Fig. 5. δ^{13}C vs δ^{18}O cross plot of the isotope ratio measurements of the benthic foraminifera, showing no statistically significant correlation.

can be used to reconstruct temperature and salinity. However, recrystallisation and/or infilling of foraminifera during diagenesis more easily affects the δ^{18}O values. This makes the use of δ^{18}O as a proxy more problematic for geochemical analyses whenever considerable diagenetic recrystallisation or overgrowth has occurred (Katz et al., 2010). In view of the fact that the foraminifera in the present study originate from Cretaceous chalk deposits that are well known for early diagenetic carbonate cementation, at least some secondary overgrowth or recrystallisation is to be expected. Several specimens of *C. bembix* were examined using scanning electron microscopy (SEM) to assess

preservation and check for overgrowth features. Furthermore, since both quarries are onshore chalk deposits, meteoric diagenesis is likely to have occurred (Hjuler, 2007), meaning the δ^{18}O values are not representative of the δ^{18}O composition of the bottom waters inhabited by the benthic foraminifera. Therefore, in the present study only the δ^{13}C measurements are used.

Results

General observations

As expected for chalk material, the sample residues are composed mainly of carbonate particles, such as foraminifera and macrofossil fragments, with very few siliciclastic mineral grains present. Nearly all samples contained fragments of echinoid spines and ostracod valves. Not a single inoceramid prism was found in the studied samples. Brachiopod and/or bivalve fragments were found in various samples from both quarries, in all members but Lixhe 1 in the ENCI quarry and in all members but Vijlen at Hallembaye. Phosphatic fish debris were found in multiple samples from all members but Vijlen at Hallembaye, but not in any of the samples from the ENCI quarry.

SEM photomicrographs

Photomicrographs of *C. bembix* show some overgrowth (Fig. 4A–E). While the broken specimens appear to be hollow, they also show some overgrowth inside the test and exhibit signs of recrystallisation (Fig. 4F). The volume of overgrowth appears relatively small compared to the volume of the test. Even though the overgrowth and recrystallisation could have slightly altered the δ^{13}C signals, the trends and general values of benthic δ^{13}C might still reflect a bottom water value, as the recrystallisation likely took place during early diagenesis on the seafloor.
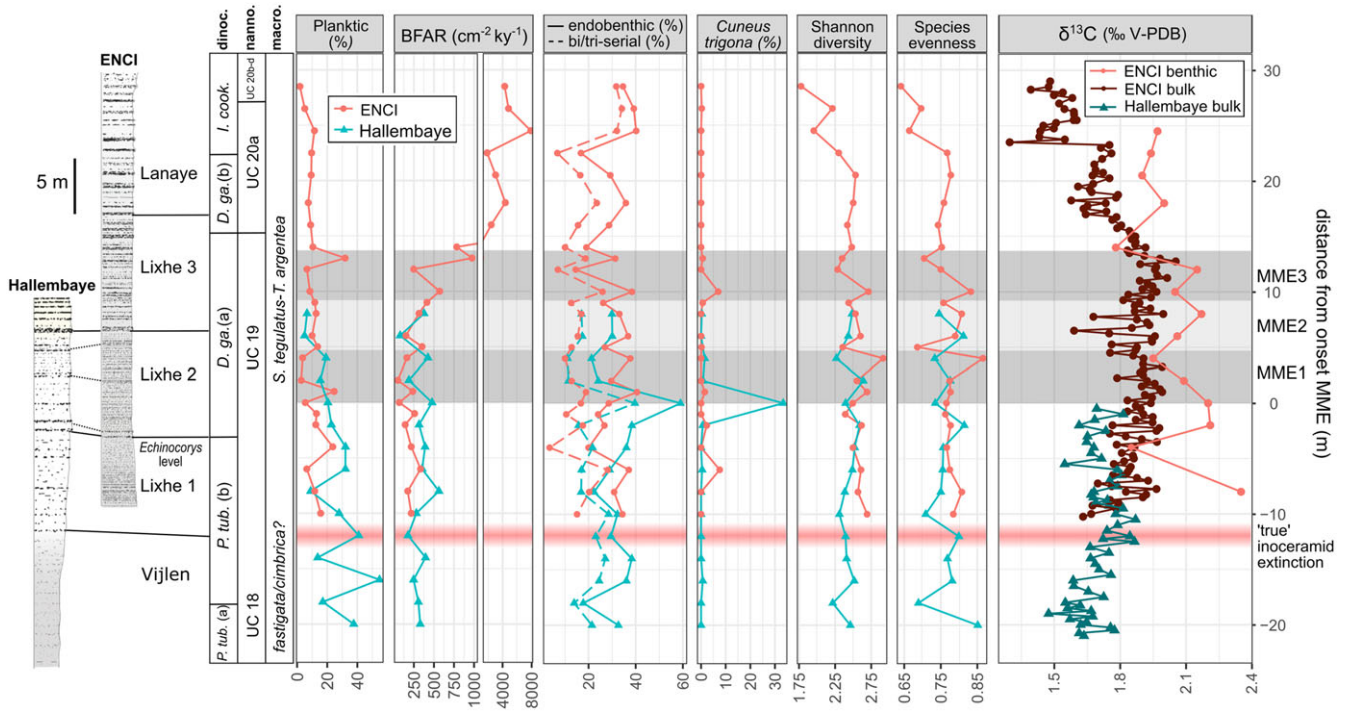
Fig. 6. Planktic percentage, benthic foraminiferal accumulation rate (BFAR), endobenthic and bi-/tri-serial foraminiferal percentage, relative abundance of Cuneus trigona, Shannon's diversity, species evenness and bulk carbonate vs benthic δ^{13}C. Biostratigraphy and bulk carbonate δ^{13}C are based on Vellekoop et al. (2022). Dinoc. = dinocysts, Macro. = macrofossil, Nanno. = nannofossil stratigraphy. P. tub. = Pervosphaeridium tubuloaculatum, D. ga. = Deflandrea galeata, I. cook. = Isabellidinium Cooksoniae, MME = mid-Maastrichtian carbon isotope event.
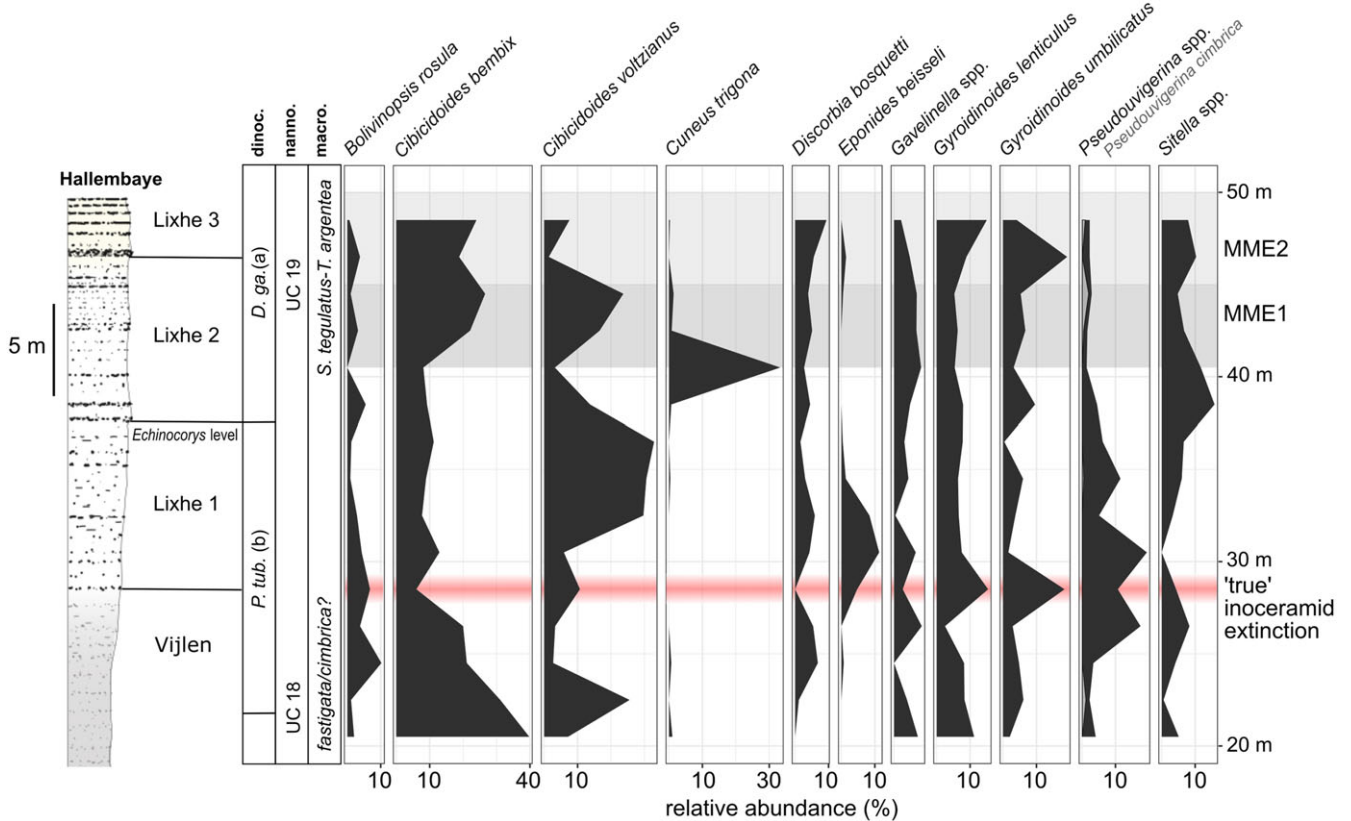

Fig. 7. Relative abundances of the most common benthic foraminifera taxa at the Hallembaye quarry. Biostratigraphy after Vellekoop et al. (2022), for abbreviations see caption of Fig. 6.
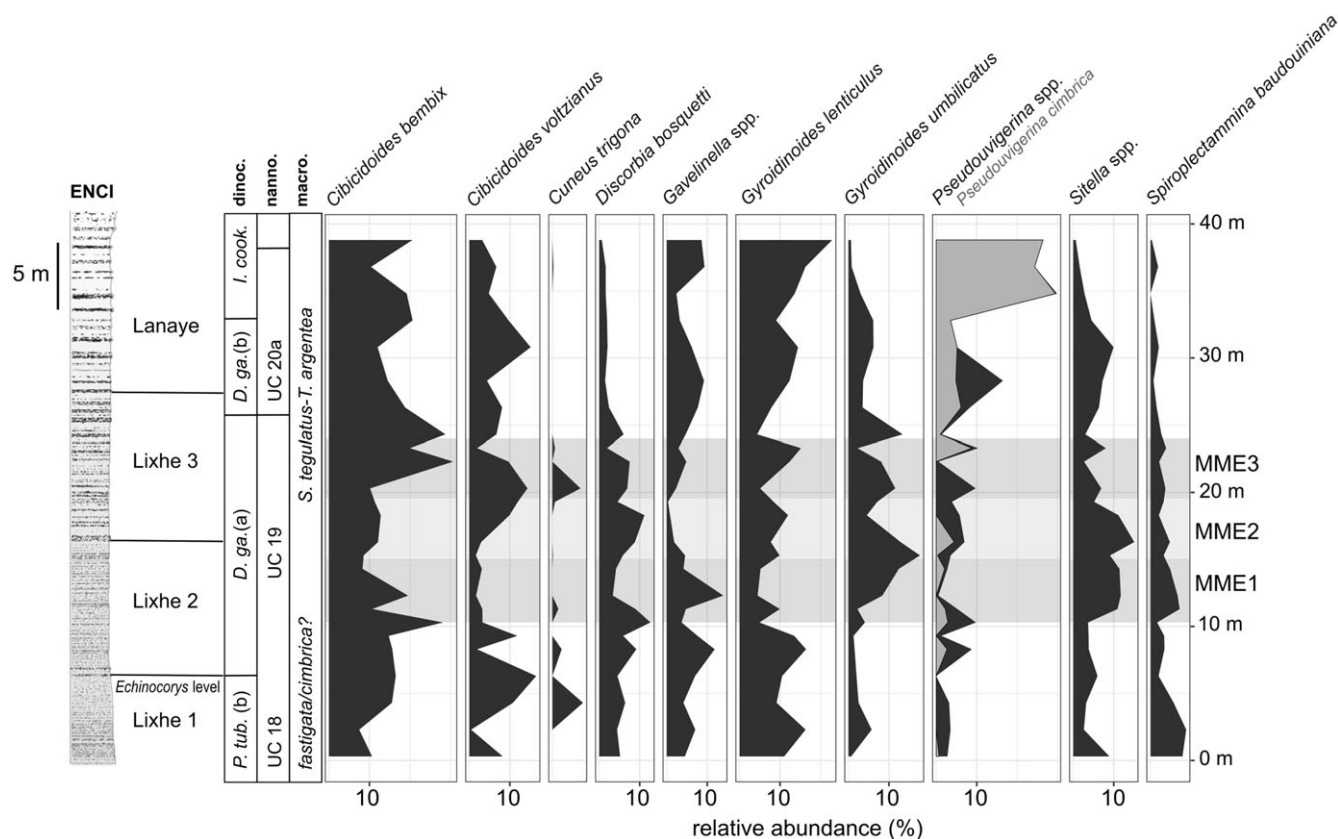
Fig. 8. Relative abundances of the most common benthic foraminifera taxa and Cuneus trigona at the ENCI quarry. Biostratigraphy after Vellekoop et al. (2022), for abbreviations see caption of Fig. 6.

Stable isotope data

The benthic δ^{13}C values vary between 1.78 and 2.35‰, while δ^{18}O values range between −2.82 and −1.19‰ (Figs. 5 and 6). A cross plot shows no statistically significant correlation between benthic δ^{18}O and δ^{13}C ($r^2 = 0.0091$, $p = 0.72$; Fig. 5), suggesting that the diagenetic overprint might be limited (Jenkyns, 1995; Mitchell et al., 1997). This would imply that the general trends in the carbon isotope record might still reflect bottom water values. In all data points except for two (ENCI_19_A_6.00 and ENCI_19_B_9.00), the benthic δ^{13}C values are higher than the bulk carbonate δ^{13}C values measured by Vellekoop et al. (2022) using the same IRMS set-up at the AMGC laboratory. While the low data resolution of the benthic δ^{13}C record does not allow the identification of an isotopic trend before the MME, during the MME the benthic δ^{13}C values appear to be closer to the bulk than after the MME (Fig. 6).

Foraminiferal assemblage data

The samples are characterised by variable preservation of foraminifera (see Tables 1 and 2). Some samples show a moderate preservation, while in other samples foraminifera exhibit clear overgrowth and recrystallisation and/or abundant broken or partially dissolved tests. The uppermost sample from Hallembaye (HAL18_B_48.50) yielded some pyritised foraminifera. Samples from just above continuous flint levels generally show poorer preservation.

There is an overall decrease in the relative abundance of planktic foraminifera across the interval, ranging from 14 to 55% in the Vijlen Member, to values around 2 to 12% in the Lanaye Member (Fig. 6). In general, small, biserial (e.g. *Heterohelix*) and

non-keeled trochospiral taxa (e.g. *Globigerinelloides*) dominate the planktic foraminiferal assemblage. At the Hallembaye quarry, samples covering the interval between 20 to 2 m below the base of the MME contain some keeled trochospiral planktic foraminifers (e.g. *Globotruncanita*), consistent with data presented by Robaszynski et al. (1985). At the ENCI quarry, some weakly keeled planktic specimens (e.g. *Globotruncanita* and *Globotruncanella*) were found in samples covering the uppermost metre of sediment of the Lixhe 3 Member and the lowest 5 m of the overlying Lanaye Member.

BFN and BFAR range between 23 and 1584 g^{-1} and 50–7887 cm^{-2}ky^{-1}, respectively (Fig. 6; supplementary files). During MME3, BFAR shows a general rise, followed by an order of magnitude increase in BFAR above the event, reaching values of 1873–4377 cm^{-2}ky^{-1} in the Lanaye Member (Fig. 6). The relative abundances of the most common taxa are shown in Figs. 7 (Hallembaye quarry) and 8 (ENCI quarry). Overall, the benthic foraminiferal assemblages appear relatively stable over the studied interval, with endobenthic taxa generally representing between 15 and 41% of the assemblage, with one outlier in the Hallembaye quarry at the onset of the MME, showing a value of 59% (Fig. 6). The Shannon diversity varies between 1.78 and 2.91, showing the highest value (2.9) within the MME interval, while the species evenness shows continuously high values (between 0.64 and 0.87) across most of the record (Fig. 6).

The epibenthic *Cibicidoides* is the most abundant genus in both quarries, generally representing 30% of the benthic foraminiferal assemblage. Other common taxa include *Gyroidinoides*, *Pseudouvigerina* and *Sitella* (Figs. 7 and 8; Plates 1–3). The onset of the MME at Hallembaye, represented by sample
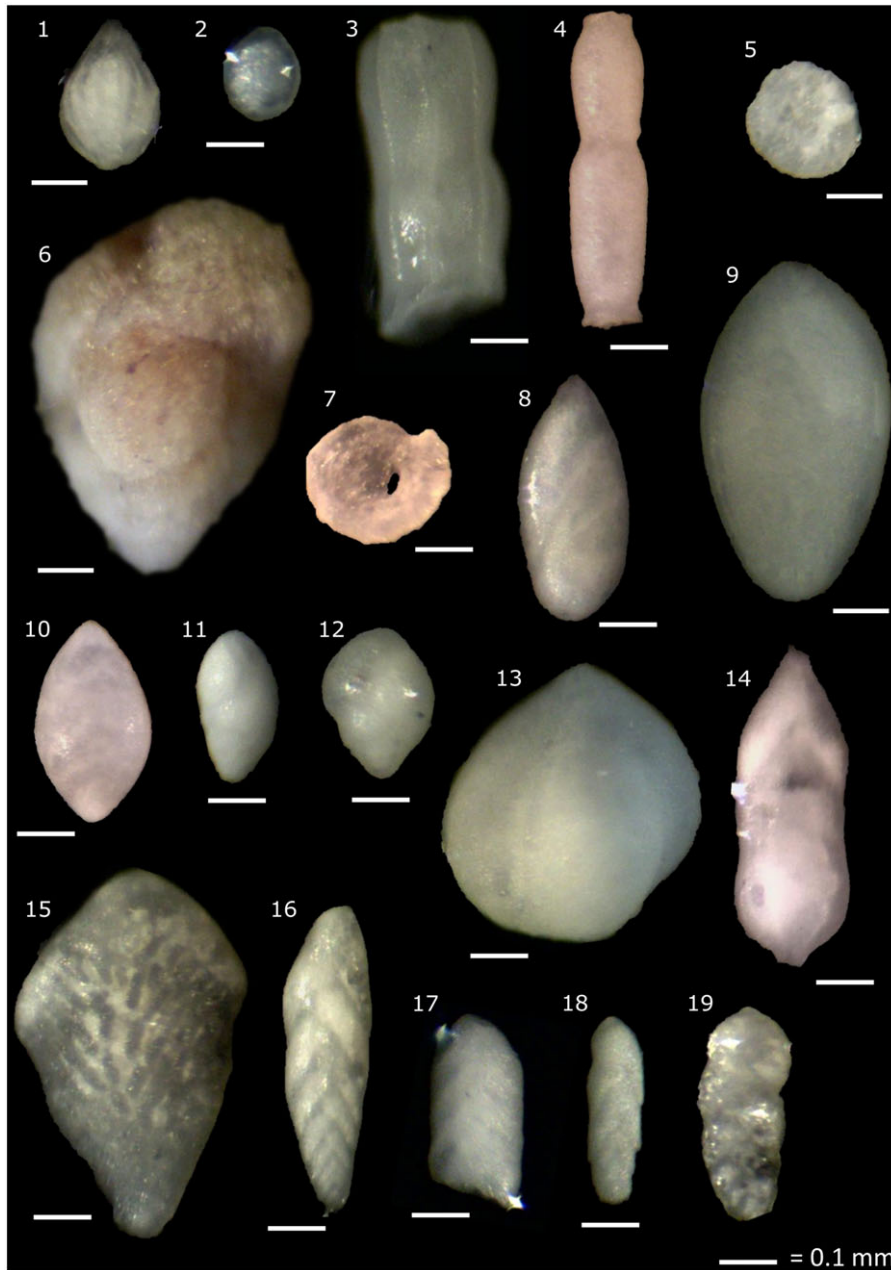
Plate 1. (1) Monothalamus costata [HAL18_A_24.50]. (2) Monothalamus smooth [ENCI_19_A_4.00]. (3) Uniserial costate [ENCI_19_A_14.00]. (4) Uniserial smooth [ENCI_19_B_7.00]. (5) Agglutinated disc [HAL18_A_24.50]. (6) Agglutinated tri-serial [HAL18_A_24.50]. (7) *Ammodiscus* sp. [ENCI_19_B_7.00]. (8) *Astacolus* sp. [HAL18_A_24.50]. (9) *Globulina* sp. [HAL18_A_36.50]. (10) *Pyrulinoides* sp. [ENCI_19_A_4.00]. (11) *Praebulimina* sp. [ENCI_19_B_7.00]. (12) *Sitella laevis* [ENCI_19_B_7.00]. (13) *Guttulina* sp. [ENCI_19_A_4.00]. (14) *Frondicularia* sp. [HAL18_A_24.50]. (15) *Bolivinoides decoratus* [ENCI_19_A_4.00]. (16) *Coryphostoma plaitum* [ENCI_19_A_4.00]. (17) *Bolivinopsis rosula* [HAL18_A_32.50]. (18) *Bolivina decurrens* [HAL18_A_36.50]. (19) *Eouvigerina cretae* [ENCI_19_A_8.00]. All scale bars represent 0.1 mm.

HAL18_A_40.50, is marked by a peak abundance of 33% of *Cuneus trigona*, an otherwise rare endobenthic species. This peak explains the anomalously high percentage of endobenthic taxa at this depth. It is not found in the ENCI quarry record (Figs. 6–8). In the Lanaye Member (ENCI) the endobenthic species *Pseudouvigerina cimbrica* shows a marked increase in abundance (Fig. 8).

Nonmetric multidimensional scaling

A nonmetric multidimensional scaling (NMDS) is performed on the relative abundance data in order to visualise changes in the benthic foraminiferal composition across the studied succession and differences between both quarries (Fig. 9). For assemblage data, NMDS is more appropriate than principal component analysis because the taxa may not have a linear response to environmental changes (Ramette, 2007). No clear distinction was observed between samples from the two quarries, nor is there a clear clustering of certain data points. The four uppermost samples from the Lanaye Member, the sample coinciding with the inoceramid extinction event and the one with a peak abundance of *Cuneus trigona* plot the furthest away from the other samples. Nevertheless, the stress value of the NMDS is higher than 0.2, indicating that
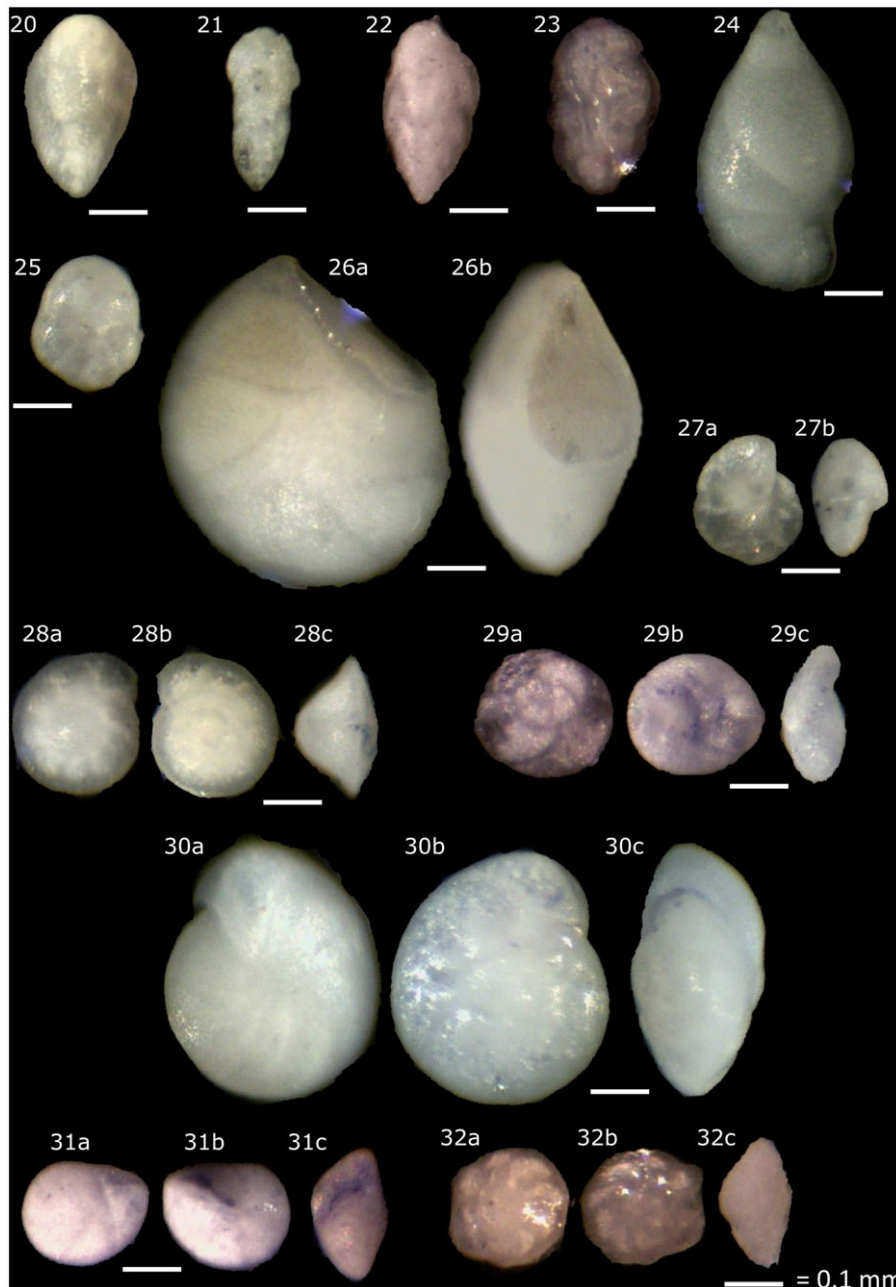
Plate 2. (20) *Cuneus trigona* [ENCI_19_A_4.00]. (21) *Cuneus minutus* [ENCI_19_A_8.00]. (22) *Pseudouvigerina cimbrica* [ENCI_19_A_8.00]. (23) *Pseudouvigerina cristata* [HAL18_A_24.50]. (24) *Saracenaria* sp. [HAL18_A_30.50]. (25) *Quadrimorphina allomorphinoides* [ENCI_19_A_4.00]. (26) *Lenticulina* sp. (lateral view, apertural view) [HAL18_A_24.50]. (27) *Pullenia* sp. (lateral view, apertural view) [ENCI_19_A_4.00]. (28) *Cibicidoides bembix* (spiral view, umbilical view, apertural view) [ENCI_19_B_7.00]. (29) *Cibicidoides dorsoconvexus* (spiral view, umbilical view, apertural view) [ENCI_19_A_4.00]. (30) *Cibicidoides voltzianus* (spiral view, umbilical view, apertural view) [HAL18_A_32.50]. (31) *Alabamina dorsoplana* (spiral view, umbilical view, apertural view) [HAL18_A_32.50]. (32) *Epistominella alata* (spiral view, umbilical view, apertural view) [ENCI_19_A_4.00]. All scale bars represent 0.1 mm.

the observed changes in benthic foraminiferal assemblages across the studied interval are not significant (Clarke, 1993).

Discussion

Benthic foraminiferal stable carbon isotopes

Remarkably, stable carbon isotope measurements at the ENCI quarry show an inverted vertical $\delta^{13}C$ gradient (Fig. 6). The bulk of the chalk consists primarily of coccoliths (calcareous nannoplankton; Haq, 1998) that lived in the pelagic zone. Bulk $\delta^{13}C$ values are therefore expected to reflect the $\delta^{13}C$ composition of the upper water column, while benthic foraminiferal $\delta^{13}C$ values document seafloor conditions. As isotopically light organic material is transported from the pelagic zone to the seafloor by the biological pump, and subsequently remineralised on the seafloor, the benthic $\delta^{13}C$ values will usually be more depleted (i.e., showing less positive values) than bulk $\delta^{13}C$ values. The record from the type-Maastrichtian shows the opposite, i.e., there is an inverted $\delta^{13}C$ gradient in the water column. A possible explanation
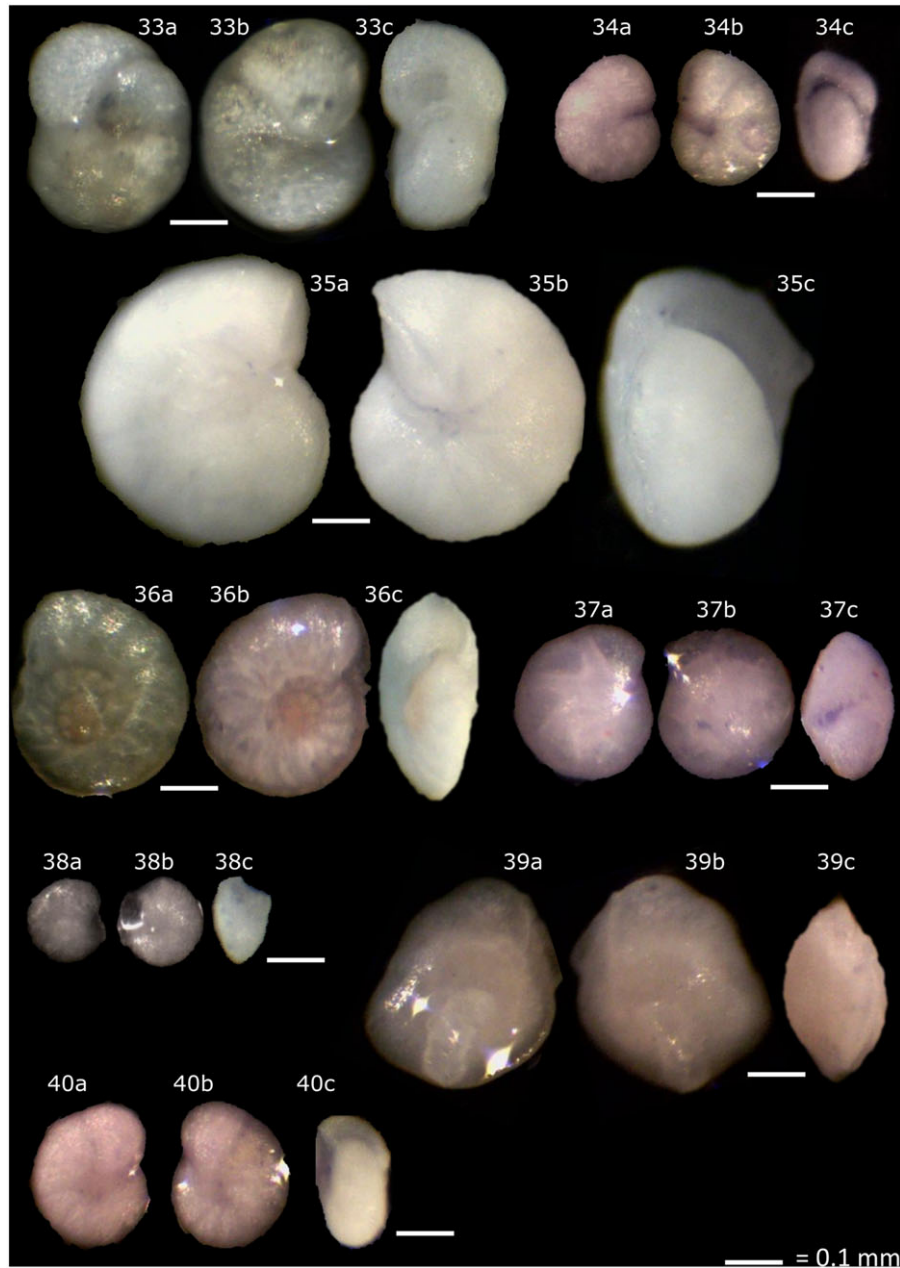
Plate 3. (33) *Discorbia bosqueti* (spiral view, umbilical view, apertural view) [ENCI_19_A_4.00]. (34) *Gyroidinoides lenticulus* (spiral view, umbilical view, apertural view) [HAL18_A_32.50]. (35) *Gyroidinoides umbilicatus* (spiral view, umbilical view, apertural view) [HAL18_A_32.50]. (36) *Gavelinella* sp. (spiral view, umbilical view, apertural view) [ENCI_19_B_7.00]. (37) *Eponides beisseli* (spiral view, umbilical view, apertural view) [HAL18_A_32.50]. (38) *Eponides* cf. *primitiva* (spiral view, umbilical view, apertural view) [ENCI_19_A_16.00]. (39) *Eponides concinna* (spiral view, umbilical view, apertural view) [ENCI_19_A_14.00]. (40) *Anomalinoides nobilis* (spiral view, umbilical view, apertural view) [HAL18_A_44.50]. All scale bars represent 0.1 mm.

is that the very fine bulk material was prone to recrystallisation during early diagenesis, thus obtaining a $\delta^{13}C$ value closer to the isotopic composition of interstitial water enriched in isotopically light carbon. This, in combination with a vital effect giving *C. bembix* a higher $\delta^{13}C$ value than the water at the seafloor, might explain the observed $\delta^{13}C$ data.

Comparison between type-Maastrichtian and the oceanic records

In contrast to considerable changes in benthic foraminiferal assemblages observed across the MME in the tropical Pacific (Frank et al., 2005; Dameron et al., 2017), the MME does not seem to have had a large impact on the seafloor conditions in the Maastrichtian type area. In these records, the MME is not marked by any remarkable changes in the foraminiferal assemblages (Figs. 7 and 8) or lithology and geochemistry of the chalk (Vellekoop et al., 2022). The only potentially significant lithological change close to the MME might be the presence of the Boirs horizon, a particularly pronounced flint band. The BFAR remains relatively constant across the inoceramid extinction level (Fig. 6), indicating no significant changes in the organic matter flux to the seafloor (Herguera, 1992). Similarly, the nearly constant species evenness close to one (Fig. 6) indicates that the benthic
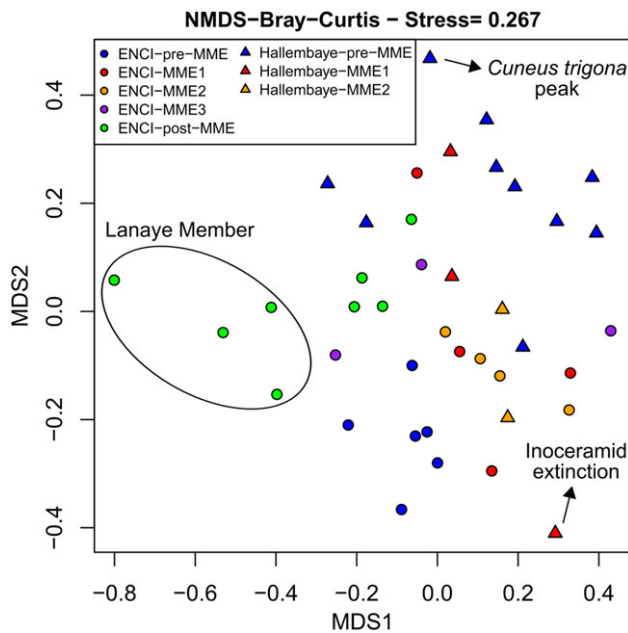
Fig. 9. Nonmetric multidimensional scaling (NMDS) of the assemblage data; the Bray-Curtis dissimilarity index was used.

environment was stable and neither oxygen nor organic matter was limiting. This is consistent with the dominance of *Cibicidoides* (Figs. 7 and 8), a genus that is indicative of well-oxygenated environments (Kaiho, 1994; Linnert et al., 2019), throughout the record. The benthic foraminiferal diversity did not decrease across the events (Fig. 6). In effect, the highest benthic foraminiferal diversity of the studied records is reached during the MME1, suggesting overall well-oxygenated and ideal trophic conditions for many species during this phase. The relatively high Mn/Al ratio throughout the succession (0.02–0.15; Fig. 10, data from Vellekoop et al., 2022) compared to the European average shale (0.01; Wedepohl, 1971) also confirms well-oxygenated conditions at the seafloor (Calvert & Pedersen, 2007). At the Hallembaye quarry, in the sample that coincides with the onset of the MME, the species *Cuneus trigona* reaches a transient peak abundance of 33.3% (Figs. 6 and 7). Potentially, it could reflect a transient change in the quantity, quality (fresh or more refractory) or timing (pulsed or constant) of the organic matter input (e.g. Jorissen et al., 2007; and references therein). This peak is not found at the nearby ENCI quarry (Figs. 6 and 8), suggesting that either the resolution of the record was too low to pick it up or that the peak at Hallembaye represents a very local event. In summary, we find no evidence that the NW-European chalk sea was influenced much by the MME. The MME was likely driven by changes in the open ocean, where also the largest ecological impacts are seen.

Nutrient recycling in the NW-European chalk sea

While neither the MME nor the extinction of 'true' inoceramids had any significant effect on the benthic environment of the shallow chalk sea in the Maastrichtian-Liège region, there is an order of magnitude increase in BFN and BFAR observed in the Lanaye Member, higher up in the stratigraphy (Fig. 6 and supplementary material). High BFARs indicate a high organic matter flux to the seafloor (Herguera, 1992). The BFN values reached in the Lanaye Member in this study (376–1585 g^{-1}) are considerably higher than most other records in the Boreal chalk sea, such as the early

Maastrichtian record from northern Germany (Friedrich et al., 2005), which shows BFN values of 30–600 g^{-1}.

The order of magnitude increase in BFN and BFAR from Lixhe 3 to the Lanaye Member (Fig. 6) coincides with a drop in relative sea level inferred by an increase in grain size and the presence of small-scale trough cross bedding (Jagt & Jagt-Yazykova, 2012; Vellekoop et al., 2022). This shallowing could have been caused by global sea level changes (Miller et al., 2003), local inversion tectonics (Bless et al., 1987; Voigt et al., 2021) and/or the infilling of the basin. While the increased BFAR indicates increased organic matter flux, major and trace element data from the same samples of the same quarry (Vellekoop et al., 2022) indicate that there was no increased terrigenous influx. Instead, the highest BFAR shows the lowest weight percentages of terrigenous elements such as Al and Ti, indicative of the influx of detrital clay from land by either riverine or aeolian processes (Vellekoop et al., 2022; Fig. 10). Therefore, the increased flux of organic matter to the seafloor, indicated by high BFAR values, must have had a different origin. Some have suggested that water mass circulation changes in the early Maastrichtian could have caused upwelling of nutrients in the NW-European shelf (Friedrich et al., 2005; Engelke et al., 2017) and that increased wind stress can increase surface water mixing which leads to higher surface water productivity (Friedrich et al., 2005). However, the sedimentation rates of the Lanaye Member are similar to those of the Vijlen and Lixhe Members (Vellekoop et al., 2022). This indicates that the nannoplankton production (which makes up the bulk of the sediment) was similar in both intervals, arguing against the hypotheses of increased surface water productivity. Alternatively, the continuous precipitation of chalk under nutrient-poor (oligotrophic to mesotrophic) conditions in the Cretaceous chalk sea (Linnert et al., 2019) was possible because of efficient nutrient recycling in the water column. In the shallower depositional setting of the Lanaye Member, nutrient recycling took place close to the seafloor, which allowed more organic matter to reach the seafloor (Fig. 11). The amount of organic matter that reaches the seafloor decreases with increasing depth, as the organic matter can be consumed by organisms in the water column (van der Zwaan et al., 1999). Similarly, in the modern oligotrophic eastern Beaufort Sea, the shallower areas have higher organic matter input at the seafloor, which is explained by the fact that the sinking organic matter has less time to be degraded (Renaud et al., 2007). We hypothesise that similar mechanisms were at play throughout the NW-European chalk sea. Our results show that quantitative benthic foraminiferal studies combined with geochemical records could provide crucial insights in the enigmatic palaeoceanography of the shallow epicontinental chalk seas.

Conclusions

Quantitative benthic foraminiferal assemblage data and a species-specific benthic stable carbon isotope record have been generated across the MME and the extinction event of non-tegulated inoceramid bivalves in the Maastrichtian type area. For this, the Maastrichtian chalk successions exposed at the Hallembaye quarry (NE Belgium) and ENCI quarry (SE Netherlands) were studied. While in deep-sea sites the MME is marked by substantial changes in benthic and planktic foraminiferal assemblages, benthic δ^{18}O values and vertical δ^{13}C gradients (Frank et al., 2005; MacLeod et al., 2005; Jung et al., 2013), the MME did not affect the epicontinental chalk sea of the type-Maastrichtian. The high and nearly constant species evenness (E) across both the MME and the
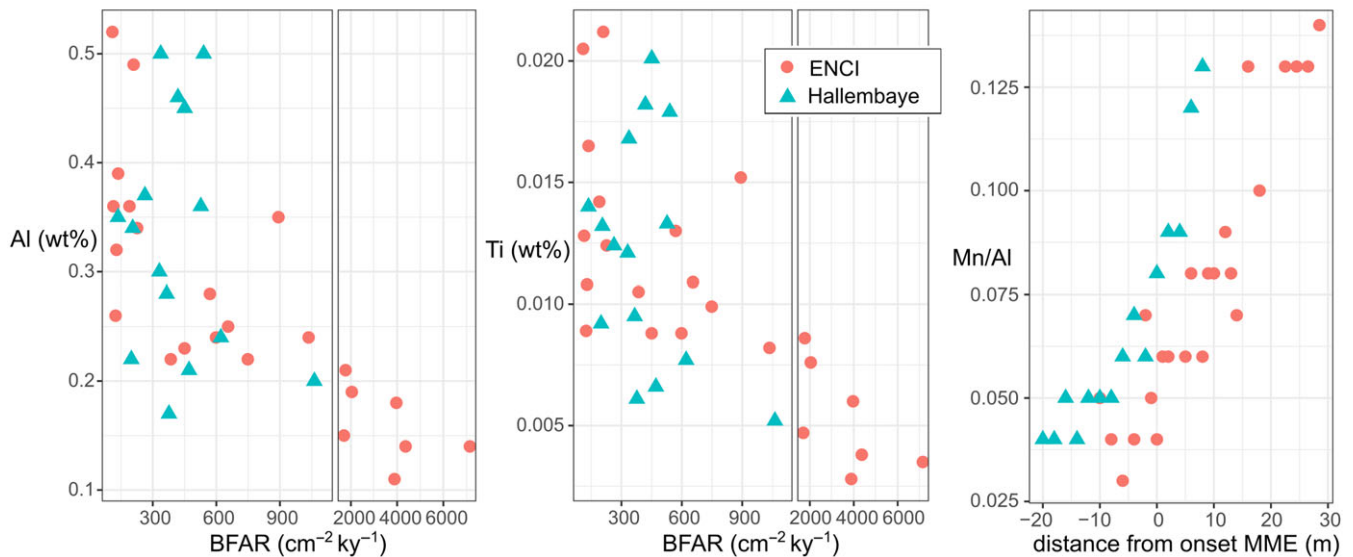
Fig. 10. Weight percentage of aluminium (Al), titanium (Ti) and manganese (Mn) in the bulk carbonate (data from Vellekoop et al., in review) vs. benthic foraminiferal accumulation rate (BFAR) and stratigraphic height.
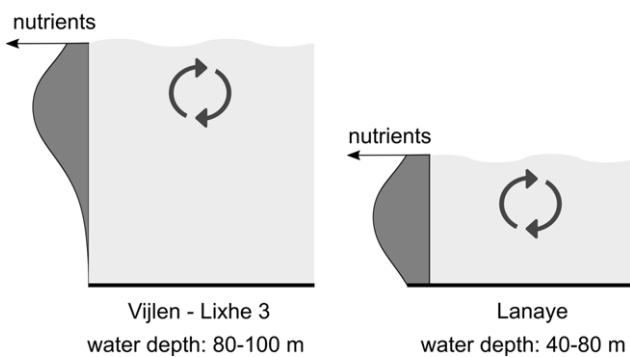

Fig. 11. Illustration of our hypothesis to explain the increased organic matter flux to the seafloor during the deposition of the Lanaye Member.

extirpation level of inoceramids shows that neither oxygen nor organic matter flux was limited during either event. At Hallembaye, the sample coinciding with the onset of the MME shows a transient peak abundance of 33.3% of the otherwise rare endobenthic species *Cuneus trigona.* This peak is likely explained by a local transient change in the organic matter flux.

While there are no clear changes in the data across the MME and the inoceramid extinction, there is an order of magnitude increase in the BFAR well after the MME. A negative correlation with terrigenous element concentrations indicates that this increased amount of nutrients at the seafloor cannot have derived from land. We hypothesise that in the deeper setting of the Vijlen and Lixhe Members efficient nutrient recycling occurred in the water column, allowing continuous chalk (calcareous nannoplankton) precipitation. In the shallower depositional setting of the Lanaye Member (above the MME), the nutrient recycling took place closer to the seafloor, allowing more organic matter to reach the seafloor, sustaining a larger benthic biomass.

References

Barrera, E., Savin, S.M., Thomas, E. & Jones, C.E., 1997. Evidence for thermohaline-circulation reversals controlled by sea-level change in the latest Cretaceous. Geology **25**: 715–718.

Bastiaans, D., Kroll, J.J.F., Cornelissen, D., Jagt, J.W.M. & Schulp, A.S., 2020. Cranial palaeopathologies in a Late Cretaceous mosasaur from the Netherlands. Cretaceous Research **112**: 104425.

Batenburg, S.J., Gale, A.S., Sprovieri, M., Hilgen, F.J., Thibault, N., Boussaha, M. & Orue-Etxebarria, X., 2014. An astronomical time scale for the Maastrichtian based on the Zumaia and Sopelana sections (Basque country, northern Spain). Journal of the Geological Society **171**: 165–180.

Batenburg, S.J., Voigt, S., Friedrich, O., Osborne, A.H., Bornemann, A., Klein, T., Pérez-Díaz, L. & Frank, M., 2018a. Major intensification of Atlantic overturning circulation at the onset of Paleogene greenhouse warmth. Nature Communications **9**: 1–8.

Batenburg, S.J., Friedrich, O., Moriya, K., Voigt, S., Cournède, C., Blum, P., Bornemann, A., Fiebig, J., Hasegawa, T., Hull, P.M., Norris, R.D., Röhl, U., Sexton, P.F., Westerhold, T., Wilson, P.A., 2018b. Late Maastrichtian carbon isotope stratigraphy and cyclostratigraphy of the Newfoundland Margin (Site U1403, IODP Leg 342). Newsletters on Stratigraphy **51**: 245–260.

Bless, M.J.M., Felder, P.J. & Meessen, J.P.M.T., 1987. Late Cretaceous sea level rise and inversion: their influence on the depositional environment between Aachen and Antwerp. In: Bless, M.J.M., Dusar, M. & Streel, M. (eds). Some aspects of the Late Cretaceous in NW Europe. Annales de la Société géologique de Belgique **109 (for 1986)**: 333–355.

Bloomfield, J.P., Brewerton, L.J. & Allen, D.J., 1995. Regional trends in matrix porosity and dry density of the Chalk of England. Quarterly Journal of Engineering Geology and Hydrogeology **28**(Supplement 2): S131–S142.

Calvert, S.E. & Pedersen, T.F., 2007. Chapter Fourteen Elemental proxies for palaeoclimatic and palaeoceanographic variability in marine sediments:

interpretation and application. *In:* Hillaire-Marcel C. & de Vernal A. (eds): Developments in marine geology (Vol. **1**). Elsevier Science (Amsterdam): 567–644.

Chauris, H., LeRousseau, J., Beaudoin, B., Propson, S. & Montanari, A., 1998. Inoceramid extinction in the Gubbio basin (northeastern Apennines of Italy) and relations with mid-Maastrichtian environmental changes. Palaeogeography, Palaeoclimatology, Palaeoecology **139**(3–4): 177–193.

Clarke, K.R., 1993. Non-parametric multivariate analyses of changes in community structure. Austral Ecology **18**(1): 117–143.

Dameron, S.N., Leckie, R.M., Clark, K., MacLeod, K.G., Thomas, D.J. & Lees, J.A., 2017. Extinction, dissolution, and possible ocean acidification prior to the Cretaceous/Paleogene (K/Pg) boundary in the tropical Pacific. Palaeogeography, Palaeoclimatology, Palaeoecology **485**(3–4): 433–454.

de Goeij, J.M., van Oevelen, D., Vermeij, M.J.A., Osinga, R., Middelburg, J.J., de Goeij, A.F.P.M. & Admiraal, W., 2013. Surviving in a marine desert: the sponge loop retains resources within coral reefs. Science **342**(6154): 108–110.

Donnadieu, Y., Pucéat, E., Moiroud, M., Guillocheau, F. & Deconinck, J.F., 2016. A better ventilated ocean triggered by Late Cretaceous changes in continental configuration. Nature Communications **7**(1): 10316.

Dubicka, Z. & Peryt, D., 2012. The Lower/Upper Maastrichtian boundary interval in the Lublin Syncline (SE Poland, Boreal realm): new insight into foraminiferal stratigraphy. Newsletters on Stratigraphy **45**(2): 139–150.

Engelke, J., Linnert, C., Mutterlose, J. & Wilmsen, M., 2017. Early Maastrichtian benthos of the chalk at Kronsmoor, northern Germany: implications for Late Cretaceous environmental change. Palaeobiodiversity and Palaeoenvironments **97**(4): 703–722.

Ernst, S.R., Guasti, E., Dupuis, C. & Speijer, R.P., 2006. Environmental perturbation in the southern Tethys across the Paleocene/Eocene boundary (Dababiya, Egypt): Foraminiferal and clay mineral records. Marine Micropaleontology **60**(1): 89–111.

Felder, P.J. & Bless, M.J.M., 1994. The Vijlen Chalk (early early to early late Maastrichtian) in its type area around Vijlen and Mamelis (southern Limburg, The Netherlands). Annales de la Société géologique de Belgique **116** (for 1993): 61–85.

Felder, W.M., 1975. Lithostratigrafie van het Boven-Krijt en het Dano-Montien in Zuid-Limburg en het aangrenzende gebied. *In:* Zagwijn W.H. & Van Staalduinen C.J (eds): Toelichting bij geologische overzichtskaarten van Nederland. Rijks Geologische Dienst (Haarlem): 63–72.

Felder, W.M., 1983. De kalksteengroeve van de cementfabriek Ciments Portland Liégeois bij Hallembaye, gem. Visé, prov. Luik, België. Grondboor & Hamer **37**: 122–138.

Felder, W.M. & Bosch, P.W., 1998. De St. Pietersberg: typelokatie van het Maastrichtien. Grondboor & Hamer **52**(Limburgnummer 9A: Geologie van de St. Pietersberg): 53–63.

Felder, W.M. & Bosch, P.W., 2000. Geologie van Nederland, deel 5. Krijt van Zuid-Limburg. NITG TNO (Delft/Utrecht): 192 pp.

Frank, T.D. & Arthur, M.A., 1999. Tectonic forcings of Maastrichtian ocean-climate evolution. Paleoceanography and Paleoclimatology **14**(2): 103–117.

Frank, T.D., Thomas, D.J., Leckie, R.M., Arthur, M.A., Bown, P.R., Jones, K. & Lees, J.A., 2005. The Maastrichtian record from Shatsky Rise (northwest Pacific): a tropical perspective on global ecological and oceanographic changes. Paleoceanography and Paleoclimatology **20**: PA1008.

Frenzel, P., 2000. Die benthischen Foraminiferen der Rügener Schreibkreide (Unter-Maastricht, NE-Deutschland). Neue Paläontologische Abhandlungen 3. Cpress (Dresden): 361 pp.

Friedrich, O. & Hemleben, C., 2007. Early Maastrichtian benthic foraminiferal assemblages from the western North Atlantic (Blake Nose) and their relation to paleoenvironmental changes. Marine Micropaleontology **62**(1): 31–44.

Friedrich, O., Herrle, J.O. & Hemleben, C., 2005. Climatic changes in the late Campanian – early Maastrichtian: micropaleontological and stable isotopic evidence from an epicontinental sea. The Journal of Foraminiferal Research **35**(3): 228–247.

Gómez-Alday, J.J., López, G. & Elorza, J., 2004. Evidence of climatic cooling at the early/late Maastrichtian boundary from inoceramid distribution and isotopes: Sopelana sections, Basque Country. Spain Cretaceous Research **25**(5): 649–668.

Hancock, J.M., 1989. Sea-level changes in the British region during the Late Cretaceous. Proceedings of the Geologists' Association **100**(4): 565–594.

Haq, B.U., 1998. Calcareous nannoplankton. *In:* Haq B.U. & Boersma A. (eds): Introduction to marine micropaleontology (Second Edition). Elsevier Science B.V. (Amsterdam): 79–107.

Herguera, J., 1992. Deep-sea benthic foraminifera and biogenic opal: glacial to postglacial productivity changes in the western equatorial Pacific. Marine Micropaleontology **19**(1–2): 79–98.

Hjuler, M.L., 2007. Diagenesis of Upper Cretaceous onshore and offshore chalk from the North Sea area. PhD Thesis. Technical University of Denmark. DTU Environment.

Huber, B.T., MacLeod, K.G. & Tur, N.A., 2008. Chronostratigraphic framework for upper Campanian-Maastrichtian sediments on the Blake Nose (subtropical North Atlantic). The Journal of Foraminiferal Research **38**: 162–182.

Jagt, J.W.M., 2001. The historical stratotype of the Maastrichtian: a review. *In:* Odin G.S. (eds): The Campanian-Maastrichtian stage boundary. Characterisation at Tercis les Bains (France) and correlation with Europe and other continents. Developments in Palaeontology and Stratigraphy 19. Elsevier Science B. V. (Amsterdam): 711–722.

Jagt, J.W.M. & Jagt-Yazykova, E.A., 2012. Stratigraphy of the type Maastrichtian – a synthesis. *In:* Jagt, J.W.M., Donovan, S.K. & Jagt-Yazykova, E.A. (eds). Fossils of the type Maastrichtian (Part 1). Scripta Geologica Special Issue **8**: 5–32.

Jagt, J.W.M. & Jagt-Yazykova, E.A., 2018. Stratigraphical ranges of tegulated inoceramid bivalves in the type area of the Maastrichtian Stage (Belgium, the Netherlands). *In*: Jagt-Yazykova, E.A., Jagt, J.W.M. & Mortimore, R.N. (eds). Advances in Cretaceous palaeontology and stratigraphy – Christopher John Wood Memorial Volume. Cretaceous Research **87**: 385–394.

Jenkyns, H.C., 1995. Carbon-isotope stratigraphy and paleoceanographic significance of the Lower Cretaceous shallow-water carbonates of Resolution Guyot, Mid-Pacific Mountains. *In:* Winterer E.L., Sager W.W., Firth J.V. & Sinton J.M. (eds): Proceedings of the ocean drilling program, scientific results. Ocean Drilling Program (College Station, TX): 99–104.

Jorissen, F.J., Fontanier, C. & Thomas, E., 2007. Paleoceanographical proxies based on deep-sea benthic foraminiferal assemblage characteristics. *In:* Hillaire-Marcel C. & De Vernal A. (eds): Developments in marine geology. Elsevier (Amsterdam): 263–325.

Jung, C., Voigt, S., Friedrich, O., Koch, M.C. & Frank, M., 2013. Campanian-Maastrichtian ocean circulation in the tropical Pacific. Paleoceanography **28**: 562–573.

Jurkowska, A. & Świerczewska-Gładysz, E., 2020. New model of Si balance in the Late Cretaceous epicontinental European Basin. Global and Planetary Change **186**: 103108.

Kaiho, K., 1994. Benthic foraminiferal dissolved-oxygen index and dissolved-oxygen levels in the modern ocean. Geology **22**: 719–722.

Katz, M.E., Cramer, B.S., Franzese, A., Honisch, B., Miller, K.G., Rosenthal, Y. & Wright, J.D., 2010. Traditional and emerging geochemical proxies in foraminifera. The Journal of Foraminiferal Research **40**: 165–192.

Keutgen, N., Jagt, J.W.M., Felder, P.J. & Jagt-Yazykova, E.A., 2010. Stratigraphy of the upper Vijlen Member (Gulpen Formation; Maastrichtian) in northeast Belgium, the southeast Netherlands and the Aachen area (Germany), with special reference to belemnitellid cephalopods. Netherlands Journal of Geosciences **89**: 109–136.

Koch, M.C. & Friedrich, O., 2012. Campanian-Maastrichtian intermediate- to deep-water changes in the high latitudes: benthic foraminiferal evidence. Paleoceanography and Paleoclimatology **27**: PA2209.

Linnert, C., Engelke, J., Wilmsen, M. & Mutterlose, J., 2019. Environmental footprints of the early Maastrichtian cooling – the record of benthic foraminifera from northern Germany. Cretaceous Research **97**: 143–159.

MacLeod, K.G., 1994. Bioturbation, inoceramid extinction, and mid-Maastrichtian ecological change. Geology **22**: 139–142.

MacLeod, K.G. & Huber, B.T., 2001. The Maastrichtian record at Blake Nose (western North Atlantic) and implications for global palaeoceanographic and biotic changes. Geological Society, London, Special Publications **183**: 111–130.

MacLeod, K.G., Huber, B.T. & Ward, P.D., 1996. The biostratigraphy and paleobiogeography of Maastrichtian inoceramids. *In:* Ryder, G., Fastovsky, D., and Gartner, S. (eds.): The Cretaceous-Tertiary event and other catastrophes in earth history. Geological Society of America, Special Paper **307**: 361–373.

MacLeod, K.G., Huber, B.T. & Isaza-Londoño, C., 2005. North Atlantic warming during global cooling at the end of the Cretaceous. Geology **33**: 437–440.

MacLeod, K.G., Isaza Londoño, C., Martin, E.E., Jiménez Berrocoso, Á. & Basak, C., 2011. Changes in North Atlantic circulation at the end of the Cretaceous greenhouse interval. Nature Geoscience **4**: 779–782.

Miller, K.G., Sugarman, P.J., Browning, J.V., Kominz, M.A., Hernández, J.C., Olsson, R.K., Wright, J.D., Feigenson, M.D. & van Sickel, W., 2003. Late Cretaceous chronology of large, rapid sea-level changes: glacioeustasy during the greenhouse world. Geology **31**: 585–588.

Mitchell, S.F., Ball, J.D., Crowley, S.F., Marshall, J.D., Paul, C.R.C., Veltkamp, C.J. & Samir, A., 1997. Isotope data from Cretaceous chalks and foraminifera: environmental or diagenetic signals? Geology **25**: 691–694.

Pielou, E.C., 1965. Species-diversity and pattern-diversity in the study of ecological succession. Journal of Theoretical Biology **10**: 370–383.

Ramette, A., 2007. Multivariate analyses in microbial ecology. FEMS Microbiology Ecology **62**: 142–160.

Renaud, P.E., Morata, N., Ambrose, W.G., Bowie, J.J. & Chiuchiolo, A., 2007. Carbon cycling by seafloor communities on the eastern Beaufort Sea shelf. Journal of Experimental Marine Biology and Ecology **349**: 248–260.

Robaszynski, F., Bless, M.J.M., Felder, P.J., Foucher, J.C., Legoux, O., Manivit, H., Meessen, J.PMTh & Van Der Tuuk, L.A., 1985. The Campanian-Maastrichtian boundary in the chalky facies close to the type-Maastrichtian area. Bulletin - Centres de Recherches Exploration-Production Elf- Aquitaine **9**: 1–113.

Shannon, C.E. & Weaver, W., 1949. The mathematical theory of communication. The University of Illinois Press (Urbana): 117 pp.

Sheldon, E., Ineson, J. & Bown, P., 2010. Late Maastrichtian warming in the Boreal Realm: calcareous nannofossil evidence from Denmark. Palaeogeography, Palaeoclimatology, Palaeoecology **295**: 55–75.

Thibault, N., Harlou, R., Schovsbo, N., Schiøler, P., Minoletti, F., Galbrun, B., Lauridsen, B.W., Sheldon, E., Stemmerik, L., Surlyk, F., 2012. Upper Campanian-Maastrichtian nannofossil biostratigraphy and high-resolution carbon-isotope stratigraphy of the Danish Basin: towards a standard d^{13}C curve for the Boreal Realm. Cretaceous Research **33**: 72–90.

van der Zwaan, G.J., Duijnstee, I.A.P., den Dulk, M., Ernst, S.R., Jannink, N.T. & Kouwenhoven, T.J., 1999. Benthic foraminifers: proxies or problems? Earth-Science Reviews **46**(1–4): 213–236.

van Hinsbergen, D.J.J., de Groot, L.V., van Schaik, S.J., Spakman, W., Bijl, P.K., Sluijs, A., Langereis, C.G. & Brinkhuis, H., 2015. A paleolatitude calculator for paleoclimate studies. PLOS ONE **10**(6): e0126946.

Vellekoop, J., Kaskes, P., Sinnesael, M., Déhais, T., Jagt, J.W.M., Claeys, P. & Speijer, R.P., 2019. The Maastrichtian Geoheritage Project: an introduction, first results and outlook. Abstract and presentation at the International Symposium on Chalk & Flint, Maastricht, The Netherlands, 30 November 2019.

Vellekoop, J., Kaskes, P., Sinnesael, M., Huygh, J., Déhais, T., Jagt, J.W.M., Speijer, R.P. & Claeys, P., 2022. A new age model and chemostratigraphic framework for the Maastrichtian type area (southeastern Netherlands, northeastern Belgium). Newsletters on Stratigraphy (Advance online publication).

Voigt, S., Gale, A.S., Jung, C. & Jenkyns, H.C., 2012. Global correlation of Upper Campanian-Maastrichtian successions using carbon-isotope stratigraphy: development of a new Maastrichtian timescale. Newsletters on Stratigraphy **45**(1): 25–53.

Voigt, T., Kley, J. & Voigt, S., 2021. Dawn and dusk of Late Cretaceous basin inversion in central Europe. Solid Earth **12**(6): 1443–1471.

Walaszczyk, I., Jagt, J.W.M. & Keutgen, N., 2010. The youngest Maastrichtian 'true' inoceramids from the Vijlen Member (Gulpen Formation) in northeast Belgium and the Aachen area (Germany). Netherlands Journal of Geosciences **89**(2): 147–167.

Wedepohl, K.H., 1971. Environmental influences on the chemical composition of shales and clays. Physics and Chemistry of the Earth **8**(1): 307–333.

Weinkauf, M.F.G. & Milker, Y., 2018. The effect of size fraction in analyses of benthic foraminiferal assemblages: a case study comparing assemblages from the >125 and >150 μm size fractions. Frontiers in Earth Science **6**: 37.